Emissivity and Growth of Auroral Kilometric Radiation in Source Regions with Perpendicular Gradients

C. J. de H. Cavalcanti, R. S. Schneider, and L. F. Ziebell
Instituto Física, Universidade do Rio Grande do Sul
Caixa Postal 15051, 91501-970, Porto Alegre, RS, Brazil

Received January 10, 1997

Emission and propagation of the auroral kilometric radiation in the auroral zones of the Earth are investigated with the use of the transfer equation for the intensity of the wave along the trajectory, which is obtained with the formulation of the geometric optics. The cyclotron emissivity and the components of the dielectric tensor are evaluated using the locally homogeneous plasma approximation, taking into account thermal effects and considering both the energetic and the background electron populations. For frequencies in the vicinity of the electron cyclotron frequency we consider a range of values of the parallel wave number which result in significant amplification. The effect of the finite width of the auroral cavities is also investigated. Our results show that the inclusion of the effect of wave emissivity along the trajectory is not sufficient to modify significatively the efficiency of the amplification.

I. Introduction

Many emission mechanism have been proposed as explanation of the auroral kilometric radiation (AKR), phenomena discovered in the late 1960s. The most commonly accepted mechanism is based in the so-called cyclotron maser instability, which assumes that the main source of energy for the amplification comes from a loss cone distribution of electrons reflected by the auroral magnetic field near the cusp regions of the Earth[1]. Also considered as relevant for the instability is the "bump" in the distribution function, a population of particles trapped by the space-varying electric field in the auroral cavity[2,3].

The cyclotron maser mechanism explains effectively the broad features of the AKR. In the investigation of more detailed features, several previous approaches to the subject of our present interest, namely the wave amplification along the trajectory of the radiation, can be found in the literature. For some of these analysis a cold plasma approximation was used in the description of wave propagation, as in the studies from the 80s which emphasized the effect of parallel gradients in the amplification (due to the sensitivity of the relativistic resonance condition to changes in the electron cyclotron frequency)[4,5]. Among other conclusions, these studies have shown that for a given frequency the maximum size of the source region of the AKR would be nearly 20 km along the magnetic field and 100 km in the perpendicular direction[5].

Another use of the cold plasma approximation utilized the transfer equation to evaluate the amplification of the AKR along the trajectory, and concluded that the maser mechanism would not be efficient to explain the observed spectral intensity of the AKR, unless that the precipitating electrons have a kinetic energy in the range 15 keV $\lesssim E_{kin} \lesssim$ 20 keV[6]. This is far beyond the observed electron energies related to AKR, as low as 4 keV[7].

These and other results have shown that thermal effects and particularly effects due to the energetic electrons could be important in the dispersion relation for electron cyclotron waves. For instance, the growth rates for the X mode can be substantially larger than those predicted by the cold plasma approximation, and the X mode cut-off frequency can be reduced to frequencies lower than the cyclotron frequency[8–13]. This downshifted cut-off frequency has indeed been observed by the Viking satellite in the auroral region[7]. Therefore, effects due to energetic electrons have also been taken into account in ray tracing analysis of wave propaga-

tion. From these ray tracing studies, it has been concluded that in the source region of AKR, at an altitude where the energetic population predominates over the cold population, extraordinary mode radiation propagates at angles very near the perpendicular to the geomagnetic field without substantial refraction, and can be amplified up to desirable levels in a path length of the order or less than 10^2 km[14].

In these applications the auroral cavity was usually considered to have a smooth density gradient in the latitudinal direction, with a scale length of $\sim 10^3$ km. Perpendicular density gradients were usually neglected, although it is now stablished the existence of cavities and density depletions in the source region[15,16,17,7,18,19]. The finite width of these auroral cavities has been considered in some situations. For instance, wave reflection at the walls of the cavity has been proposed as a feedback mechanism which would produce wave amplification[20]. Also in simulations the finite width of the source region has been included, as in the case of a one-dimensional simulation in which only the perpendicular coordinate was considered and the magnetic field was assumed to be uniform[21]. The radiation has been assumed restricted to perpendicular propagation, resulting significant increase in the efficiency of the amplification as compared to other simulations where the source region was treated as infinite by means of periodic boundary conditions[21].

In our first approach to the study of propagation and amplification of the AKR, we utilized the Poeverlein method for the wave trajectory, taking into account perpendicular gradients and the finite width of the source region[22]. The conclusion has been that the effect of perpendicular gradients in the auroral cavities is such that it causes increase in the wave amplification, as compared to cavities with infinity width[22]. We later on improved the description of the wave trajectory by the development of a full ray tracing code which used the formalism of the geometrical optics, keeping thermal and relativistic effects in the dispersion relation. An analysis made with this code has shown that, although the finite size of the auroral cavities may contribute to enhance the level of the AKR radiation, it is not as effective as indicated by the previous approach which used the method of Poeverlein[23].

More recently, we introduced a development in the ray tracing treatment, by the evaluation of the emissivity along the trajectory, and the use of the transfer equation in order to obtain the wave amplitude at each point. The formalism has been applied to the study of wave propagation inside auroral cavities featuring internal density depletions[24]. These internal depletions have been reported in the literature[25,19], and are modelled in our study by the use of a model profile for the plasma parameters in the cavity.

In the present paper we report on an application of the same formalism to the case of a single cavity, in order to study the effect of the cavity width on the emissivity and on the final level of wave amplification. We consider waves with frequency in the vicinity of the electron cyclotron frequency, and a range of wave numbers around the most unstable wave number at the initial position, for a given frequency.

The plan of the paper is the following: In Sec. II we describe the physical model utilized for the source region. In Sec. III we present a brief summary about the theoretical framework utilized, including the dispersion relation for electromagnetic waves, the electronic emissivity, and the equations for the ray trajectory and the transfer equation. In Sec. IV we present the results of a numerical analysis, emphasizing the effect of the finite width of the source region on the emissivity and on the final level of the AKR radiation. Sec. V summarizes and discusses the results obtained.

II. The model for the source region

As in our previous applications the plasma in the source region is considered to be constituted of several populations, including hot plasma of magnetospheric origin, cold plasma of ionospheric origin, backscattered electrons from the ionosphere, and trapped electrons due to the electric field and magnetic mirrors. The densities, the drift velocities, and the temperatures of these plasma populations are evaluated at each point with the use of a model which provides the profiles for these quantities, between two points along the geomagnetic field lines, called the source points[26]. One of the source points is at the top of the ionosphere, approximately at 100 km above the surface of the Earth, at the altitude where the frequency of collisions between the particles matches the electron cyclotron frequency. The other point is situated at the magnetic equator, where the hot plasma is injected from.

In our study we consider only the radial variation of the geomagnetic field. The latitudinal dependence is ignored because we are interested only in the portion of the ray path where amplification occurs, restricted to a

distance of a few hundreds of km. The field is therefore given by $B_s = 0.6/z_s^3$ G, where z_s is the altitude of the point s in Earth's radii. The cavity with finite width is simulated by the introduction of the dependence of the total electronic density in the perpendicular direction, x, as follows

$$n_{Te}(x,s) = \bar{n}_{Te}(s)[\Delta - (\Delta - 1)e^{-(x/L_x)^2}] \,,$$

where $\bar{n}_{Te}(s)$ is the total electronic density at the center, $\Delta\bar{n}_{Te}(s)$ is the total density at the border, Δ is a real number greater than one, and L_x is a parameter that measures the width of the cavity. Temperature and drift velocity are described by exponentially decreasing profiles[22].

The actual electron distribution function measured in the source region features a one-sided loss cone and the "bump" due to trapped particles as prominent characteristics, along with the drift velocity of the magnetospheric electrons, v_d. For waves with frequency larger than the electron cyclotron frequency, and for $0 \leq N_\parallel < 1$, the resonant curve is an ellipse localized in the region of positive parallel velocities. In this case, it has been shown that the growth rates for fast extraordinary mode waves are relatively insensitive to details of the distribution function, as long as it exhibits a loss cone feature[8]. Taking into account these considerations, we use a two-sided drifting loss cone as a model distribution for the magnetospheric electrons, and write the total distribution as a sum of two populations, a hot loss cone plus a cold Maxwellian background:

$$n_{Te} f_0(\vec{u}) = n_{Me} f_{LC}(\vec{u}) + (n_{Te} - n_{Me}) f_M(\vec{u}),$$

where n_{Me} is the density of loss cone magnetospheric electrons, and both $f_{LC}(\vec{u})$ and $f_M(\vec{u})$ are given by the following distribution function[27]:

$$f_\alpha(\vec{u}) = A_\alpha u_\perp^{2l_\alpha} e^{-\gamma_\alpha \mu_\alpha(\gamma - \beta_\alpha u_\parallel)} \qquad (1)$$

with $A_\alpha = \mu_\alpha^{l_\alpha+1}/(4\pi 2^{l_\alpha} l_\alpha! \gamma_\alpha K_{l_\alpha+2}(\mu_\alpha))$, $\mu_\alpha = m_e c^2/T_\alpha$, $\gamma = (1+u^2)^{1/2}$, $\beta_\alpha = v_\alpha/c$, where v_α is the drift velocity of the species labelled by $\alpha, \gamma_\alpha = (1-\beta_a^2)^{-1/2}$, and l_α is a positive integer, known as loss cone index, and K_n is a modified Bessel function of second kind. For $\alpha = LC, l_{LC} \geq 1$ and for $\alpha = M, l_M = 0$. Since $\beta_M = 0$, in what follows we denote β_{LC} as β_d, and γ_{LC} as γ_d, for simplicity. A contour plot of the distribution function, evaluated at the center of an auroral cavity at $z = 2.5\ R_\oplus$, for $l_{LC} = 2$, can be found in our previous ray tracing calculation on the AKR propagation and amplification[23].

III. The theoretical framework

The auroral region is described by a two-dimensional plasma slab, with the z axis pointing upward along the geomagnetic field, the x axis along the magnetic latitudinal direction, and the slab considered to be homogeneous in the y direction.

III.1 The dispersion relation

With the geometry utilized, the dispersion relation for electromagnetic waves may be written as follows

$$\Lambda(\vec{k},\omega,x,z) = AN_\perp^4 + BN_\perp^2 + C = 0 \qquad (2)$$

where

$$\begin{aligned}
A &= (1+\chi_{11})(1-\chi_{33}) + \chi_{13}(2N_\parallel + \chi_{13}) + \chi_{33}N_\parallel^2 \\
B &= (\chi_{11}+1-N_\parallel^2)[\chi_{23}^2 - 1 - e_{zz} + \chi_{33}(\chi_{22}+1-N_\parallel^2)] \\
&- (\chi_{22}+1-N_\parallel^2)[1+\chi_{11}+\chi_{13}(2N_\parallel+\chi_{13})] - \chi_{12}^2(1-\chi_{13}) + 2\chi_{12}\chi_{23}(N_\parallel+\chi_{13}) \\
C &= (1+e_{zz})[(\chi_{11}+1-N_\parallel^2)(\chi_{22}+1-N_\parallel^2) + \chi_{12}^2] \,.
\end{aligned}$$

$N_\perp$ and $N_\parallel$ are respectively the perpendicular and parallel components of $\vec{N} = c\vec{k}/\omega$, where $\vec{k}$ is the wave vector. The indexes (1, 2, 3) are used as equivalent to (x, y, z).

Explicit expressions for the χ_{ij} components and for e_{zz} can be found elsewhere, both in general form, and particularized for the case of the distribution function (1) [22, 23]. The χ_{ij} components are part of the dielectric tensor components, and defined as follows

$$\epsilon_{ij} = \delta_{ij} + \delta_{iz}\delta_{jz}e_{zz} + N_\perp^{\delta_{iz}+\delta_{jz}}\chi_{ij}. \qquad (3)$$

III.2 The emissivity

The spectral emissivity $\eta(\omega, N_\parallel)$ can be defined as follows[24]

$$\eta(\omega, N_\parallel) = \frac{d^2\hat{P}_{av}}{dN_\parallel d\omega}\ , \qquad (4)$$

where $\hat{P}_{av}$ is the average power radiated per unit of volume. Using an analytical development which will not be repeated here, since it can be easily found in the literature[28,29], and considering the case of the model distribution function (1), it is straightforward to obtain from this general definition the following expression for the spectral emissivity for a given wave mode, for electrons of species α [24],

$$\begin{aligned}\eta_\alpha(\omega, N_\parallel) &= X_\alpha \frac{\omega^3}{c^3} A_\alpha m_e c^2 \frac{N_\perp}{|\partial_{N_\perp}\Lambda_r(\omega, N)|}\sum_{n=1}^{\infty}\int_{u_-}^{u_+} du_\parallel [\bar{\gamma} - 1 - u_\parallel^2]^{l_a+1} \\ &\times\ e^{-u_\alpha\gamma_\alpha[\bar{\gamma}-\beta_a u_\parallel]}[\xi_{ni}^*\lambda_{ij}(\omega, N)\xi_{nj}], \qquad (5)\end{aligned}$$

where

$$\xi_n = \left[\frac{n}{\bar{b}}J_n(\bar{b}), iJ_n'(\bar{b}),\ \frac{N_\perp u_\parallel}{Y\bar{b}}J_n(\bar{b})\right]\ ,$$

and

$$u_\pm = \frac{nN_\parallel Y \pm \sqrt{n^2Y^2 - 1 + N_\parallel^2}}{(1 - N_\parallel^2)}\ .$$

The 'overline' symbol means that the quantity has been evaluated over the resonance curve, given by $\bar{\gamma} = nY + N_\parallel u_\parallel$, where $Y \equiv |\Omega_e|/\omega$. We have defined $X_\alpha = \omega_{p\alpha}^2/\omega^2$, where $\omega_{p\alpha}^2 = 4\pi n_\alpha q_a^2/m_\alpha$ is the squared plasma frequency of species α (same notation employed in the explicit expressions for the dielectric tensor components[22,23]), with n_α being the particle density of species α. J_n and J_n' are respectively the Bessel function and its derivative, of argument $b = k_\perp u_\perp/|\Omega_e|$, where $\Omega_e \equiv -eB_0/(m_e c)$. For practical use, only the harmonic $n = 1$ has been considered in the calculation, and only the first relevant term has been used after expansion of the Bessel functions. The quantity $\Lambda_r(\omega, N)$ is the real part of the dispersion relation, obtained with the use in (2) of the hermitian parts of the dielectric tensor components.

III.3 The ray tracing procedure and the transfer equation

Using the conventional approach to the geometric optics, valid whenever the anti-hermitian parts are much smaller than the hermitian parts[30], we obtain the trajectory of the waves as a solution for the following equations.

$$\frac{dx}{dt} = -\partial_{k_x}\Lambda_r/\partial_\omega\Lambda_r\ ,\ \frac{dk_x}{dt} = \partial_x\Lambda_r/\partial_\omega\Lambda_r$$

$$\frac{dz}{dt} = -\partial_{k_z}\Lambda_r/\partial_\omega\Lambda_r\ ,\ \frac{dk_z}{dt} = \partial_z\Lambda_r/\partial_\omega\Lambda_r \qquad (6)$$

After tedious calculations which make explicit use of the dispersion relation and the expression for the components of the dielectric tensor, these equations are reduced to a set of coupled equations which are dependent on the χ_{ij} and its derivatives[23]. These coupled differential equations are then solved numerically by means of a Runge-Kutta method with adaptative time step[31], providing the wave trajectory.

The intensity of radiation along the wave trajectory is obtained from the transfer equation,

$$\frac{d}{ds}\left(\frac{I_\omega}{N_r^2}\right) = -\alpha\left(\frac{I_\omega}{N_r^2}\right) + \frac{\eta(\omega,\theta)}{N_r^2} = -\alpha\left(\frac{I_\omega}{N_r^2}\right) + \frac{\eta(\omega,N_\parallel)\cos\beta}{2\pi N} \tag{7}$$

where I_ω is the intensity of the radiation, α is the absorption coefficient, which can be given by $\alpha = -2k''_\perp$, N_r is the so-called 'ray refraction index', N is the absolute value of the refraction index, and $ds = \sqrt{dx^2 + dz^2}$ is an element of the wave trajectory[32]. The real and imaginary parts of $N_\perp$ are denoted respectively as $N'_\perp$ and $N''_\perp$, and therefore $k''_\perp = (\omega/c)N''_\perp$. The spectral emissivity $\eta(\omega, N_\parallel)$ results from the addition of the emissivities due to all species of particles, $\Sigma_\alpha \eta_\alpha$. We have taken into account the factor $N/(2\pi)$ which comes from the change of variable between θ and $N_\parallel$, where θ is the angle between the direction of the wave vector and the magnetic field. We have also taken into account the difference between the elements of solid angle relative to the direction of $\mathbf{k}$ and the direction of the energy flux[33,34],

$$\frac{d\Omega_{\mathbf{k}}}{d\Omega_{\mathbf{S}}} = \left(\frac{N_r}{N}\right)^2 \cos\beta \ ,$$

where

$$\tan^2\beta = \left(\frac{N_\perp \partial_{N_\parallel}\Lambda - N_\parallel \partial_{N_\perp}\Lambda}{N_\perp \partial_{N_\perp}\Lambda + N_\parallel \partial_{N_\parallel}\Lambda}\right)^2 \ ,$$

where β is the angle between the directions of $\mathbf{k}$ and the energy flux. For the cases considered in what follows, the value of $\cos\beta$ never departs much from unity, with small effect on the amplification factor. The formal solution of the transfer equation may be given by the following expression

$$I_\omega(s) = e^{-2\int_{x_0}^{x} dx' k''_\perp(x')}\left[I_\omega(x_0) + \int_{s_0}^{s} ds' \frac{\eta(\omega,N_\parallel)\cos\beta}{2\pi N} e^{2\int_{x_0}^{x'} dx'' k''_\perp(x'')}\right] \ , \tag{8}$$

which gives the wave intensity at position s, after integration between the starting position (s_0) and position s, along the trajectory which is the outcome of the numerical solution of Eqs. (6) [24].

IV. Numerical analysis and results

For the magnetospheric model, we assume the following boundary conditions: $V_l = 8$ kV, $N_{Me} = 0.8$ el/cm^3, $T_{\parallel e} = 4$ keV, and $T_{\perp e} = 6$ keV, which are the same as those from "model B" in our previous ray tracing study, with the same value for the loss cone index, $l_{LC} = 2$ [23]. In addition, we assume $L = 500$ km as the cavity width, $\Delta = 10$, and $T_M = 0.1$ eV as the cold background temperature.

We therefore follow the trajectory of waves with angular frequency $\omega = 1.008|\Omega_e|$, starting from position $z_0 = 2.5R_\oplus$ with a range of values of $N_\parallel$. In Fig. 1 we show the value of $N'_\perp$ as a function of the initial values of $N_\parallel$ and the time since the departure of the waves from the center of the cavity. Since the starting value of N is around unity, the range of values of $N_\parallel$ considered is related to a bunch of rays propagating at an angle $\simeq 80°$ relative to the magnetic field, with an angular width of $\simeq 3°$.

In Fig. 2 we show the values of $N''_\perp$ vs. time and $N_\parallel$, for the same frequency. It is seen that those rays in the lower end of the $N_\parallel$ range are barely amplified at the starting position, experiment significant values of the negative absorption coefficient along the trajec-

tory, and finally leave the resonant region ($N_\perp''$ vanishes asymptotically). The rays in the upper end of the $N_\parallel$ range find significant negative values of $N_\perp''$ in the beginning of the trajectory, but suffer positive absorption in the later stages of the propagation.

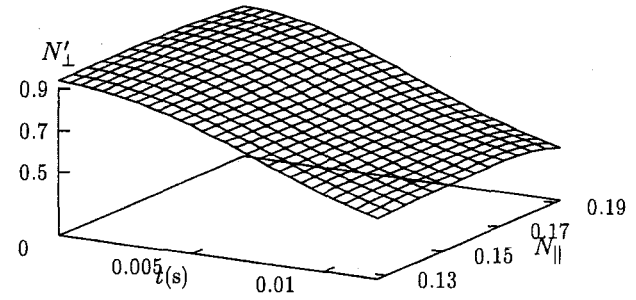

Figure 1. $N_\perp'$ as a function of the initial values of $N_\parallel$ and the time since the departure of the wave from the center of the cavity, for $\omega = 1.008\ |\Omega_e|$; $z_0 = 2.5R_\oplus$, $\Delta = 10$, and $L = 500$ km.

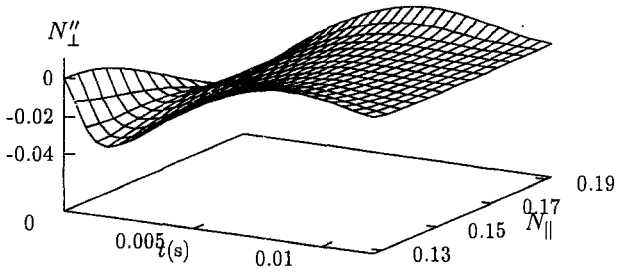

Figure 2. $N_\perp''$ as a function of the initial values of $N_\parallel$ and the time since the departure of the wave from the center of the cavity, for $\omega = 1.008\ |\Omega_e|$; other parameters as in Fig.1.

The spectral emissivity as a function of time and $N_\parallel$ is seen in Fig. 3. We have explored the frequency dependence of the emissivity, by considering three values of wave frequency. Panels (a), (b), and (c) of Fig. 3 display respectively the cases of $\omega = 1.005|\Omega_e|$, $1.008\ |\Omega_e|$, and $1.011\ |\Omega_e|$. Panel (a) shows that the emissivity for the frequency closer to the electron cyclotron frequency grows along propagation, starting from small values and finishing by being negligible, with a quite uniform behaviour for the whole range of $N_\parallel$. For the case of the intermediate frequency $\omega = 1.008\ |\Omega_e|$ the emissivity is initially more significant in the upper range of $N_\parallel$, grows along the trajectory, and also vanishes at the end of the trajectory. Similar behaviour, with more pronounced asymmetry between the lower and upper ranges of $N_\parallel$, is seen for $\omega = 1.011\ |\Omega_e|$ in panel (c) of Fig. 3.

Figure 3 (a)

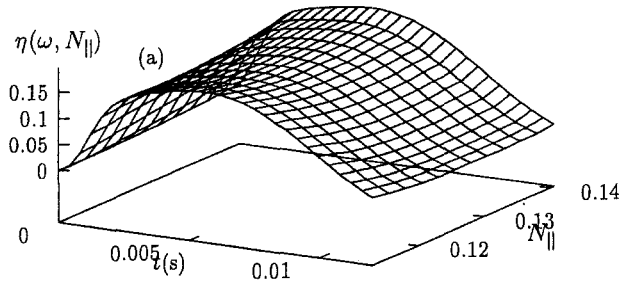

Figure 3 (b)

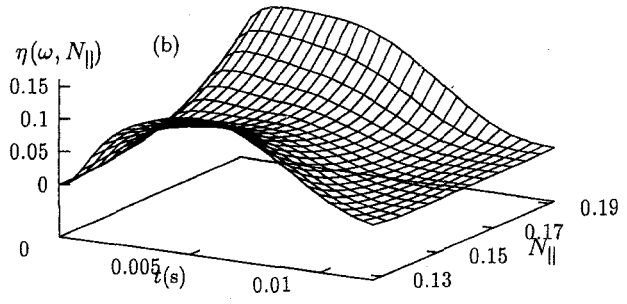

Figure 3 (c)

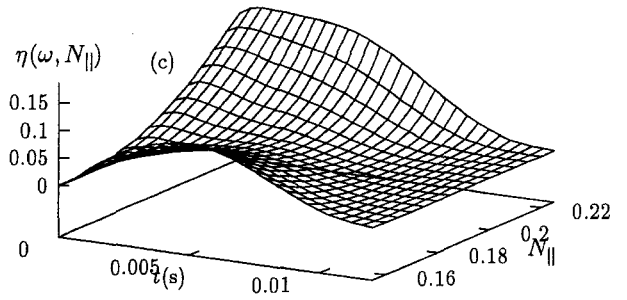

Figure 3. $\eta(\omega, N_\parallel)$ as a function of the initial values of $N_\parallel$ and the time since the departure of the wave from the center of the cavity, for three values of the wave frequency and other parameters as in Fig. 1. (a) $\omega = 1.005\ |\Omega_e|$; (b) $\omega = 1.008\ |\Omega_e|$; (c) $\omega = 1.011\ |\Omega_e|$.

Figure 4 (a)

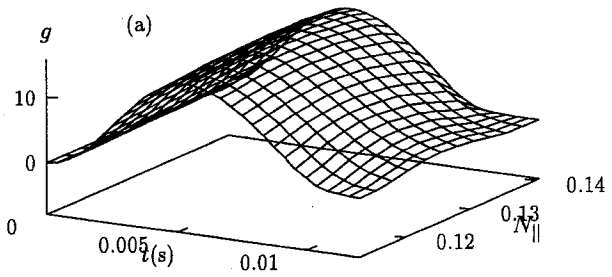

Figure 4 (b)

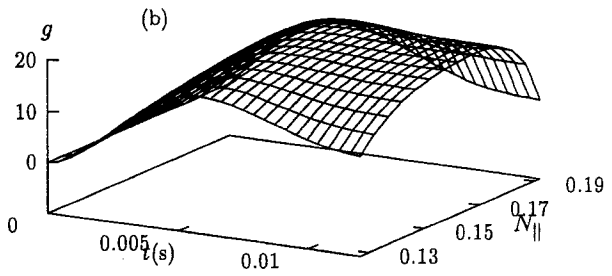

Figure 4 (c)

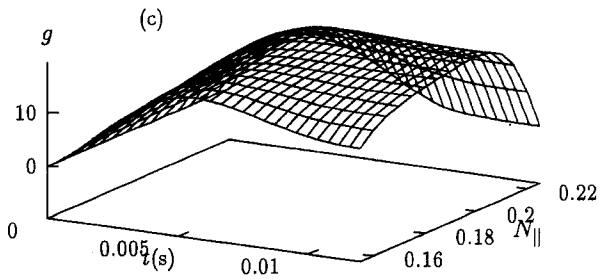

Figure 4. $g \equiv ln(I_\omega/I_{bb})$ as a function of the initial values of $N_{||}$ and the time since the departure of the wave from the center of the cavity, for three values of the wave frequency and other parameters as in Fig. 1. (a) $\omega = 1.005\ |\Omega_e|$; (b) $\omega = 1.008\ |\Omega_e|$; (c) $\omega = 1.011\ |\Omega_e|$.

Figure 5

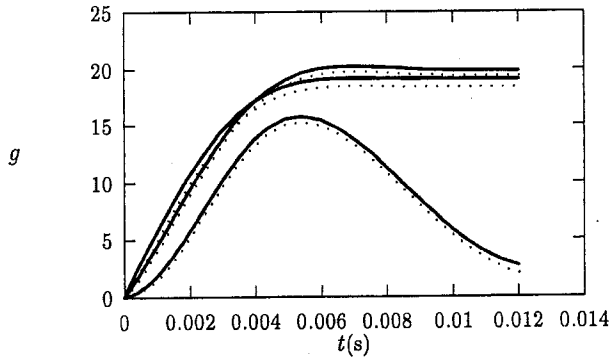

Figure 5. g for the most amplified values of $N_{||}$ for the frequencies $\omega = 1.005$, 1.008, and 1.011 $|\Omega_e|$ as a function of time since the departure from the center of the cavity. The dotted lines in each case indicate the values of g obtained when $\eta(\omega, N_{||})$ is assumed to be zero.

In order to evaluate the intensity of the wave along the trajectory we have used Eq. (8), assuming the wave level at the starting point of the ray tracing procedure as being equal to the intensity of black body radiation, $I_{bb} = \omega^2 T_e/(8\pi^3 c^2)$. In Fig. 4 we show the natural logarithm of I_ω/I_{bb}, refered in what follows as the 'amplification factor' g, vs. $N_{||}$ and the time. The case of $\omega = 1.005\ |\Omega_e|$ is seen in panel (a) of Fig. 4. The range of values shown covers the maximum amplification for this frequency. The whole range of $N_{||}$ displays amplification along the trajectory and is later on partially reabsorbed, with the ray close to the center being the most amplified at the end of the resonance region ($N_{||} \simeq 0.13$). For this frequency very close to the electron cyclotron frequency, therefore, wave amplification by the loss cone mechanism is negligible in the proposed cavity. In panel (b) of Fig. 4 one sees the case of $\omega = 1.008\ |\Omega_e|$. The maximum amplification is near the middle of the range of $N_{||}$, for initial value of $N_{||} \simeq 0.16$. The level of amplification attained for the most amplified rays is significant, since it corresponds to a final intensity level nearly 4×10^8 times the initial level. The case of $\omega = 1.011\ |\Omega_e|$ appears in panel (c) of Fig. 4. It is seen that the maximum amplification occurs for initial value of $N_{||}$ nearly $N_{||} = 0.19$, with the amplification level already slightly smaller than in the case of $\omega = 1.008\ |\Omega_e|$. The conclusion is that waves with frequency $\omega \simeq 1.01\ |\Omega_e|$ are the most amplified in the cavity, with an amplification factor of $\simeq e^{20}$, for the parameters utilized. This is significant, corresponding to nearly 87 db, but still insufficient to account for the ob-

served levels of AKR. Incidentally, we remark about a mistake about the parameters utilized in Fig. 10 of [23]. In the caption of that figure it is said that the values of $N_{||}$ utilized are those which give maximum amplification rate at the starting position, for the frequencies considered. We found out that this is not really the case for the parameters considered. Those values of $N_{||}$ should be therefore regarded as examples of values of $N_{||}$ which give significant amplification rate, and not necessarily as the most amplified at the starting position.

In Fig. 5 we compare the cases of the most amplified values of $N_{||}$ for the three frequencies considered, with values of amplification obtained without taking into account the emissivity along the ray; that is, values obtained from the use of Eq. (8) with $\eta = 0$. It is seen that the addition of the spectral emissivity along the trajectory does not change qualitatively the amplification of the wave, and that the quantitative change is not significant, being responsible at most for a factor of 2 in the final intensity for the most amplified rays. The effect is more significant for values of $N_{||}$ which are less amplified, specially those which suffer absorption before leaving the cavity. For instance, for the ray with $\omega = 1.005\ |\Omega_e|$ and $N_{||} = 0.113$, panel (a) of Fig. 4 shows very small amplification at the end of the computed trajectory. If the emissivity is neglected along the ray-tracing, the amplification would be negative for this ray. Therefore, the inclusion of the emissivity along the ray has significant effect in this case, but the amount of amplification is nevertheless negligible.

The effect of the width of the cavity on the cyclotron emissivity along the trajectory is shown in Fig. 6, for the case of $\omega = 1.008\ |\Omega_e|$. Panel (a) shows η vs. $N_{||}$ and vs. time, for $L = 400$ km, while panel (b) shows the case of $L = 300$ km. These curves should be compared with panel (b) of Fig. 3, which exibits the case of $L = 500$ km. The reduction of the cavity width causes an increase in the emissivity for the frequency considered, but the amplification is indeed reduced[23]. Panels (a) and (b) of Fig. 7 show the values of $N''_{\perp}$ vs. $N_{||}$ and time, for $\omega = 1008\ |\Omega_e|$ and $L = 400$ km and $L = 300$ km, respectively. By comparing these panels with Fig. 2, it is seen that, although the amplification rate can increase along the trajectory for some values of $N_{||}$, with the decrease of L all the range of $N_{||}$ considered suffers absorption before leaving the cavity. The overall effect is seen in Fig. 8, where we show the value of g along the trajectory, for $L = 400$ km (panel (a)) and $L = 300$ km (panel(b)).

Figure 6 (a)

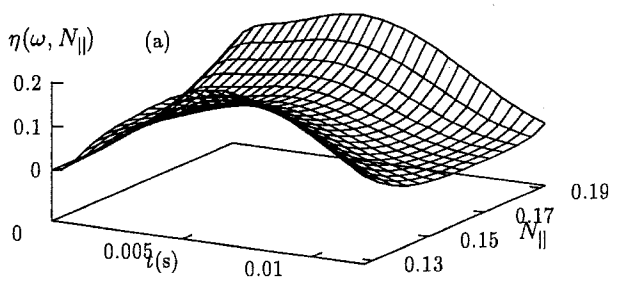

Figure 6 (b)

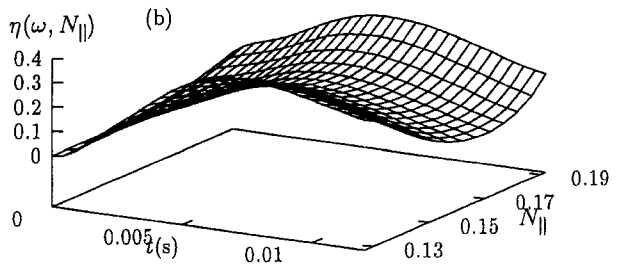

Figure 6. $\eta(\omega, N_{||})$ as a function of the initial values of $N_{||}$ and the time since the departure of the wave from the center of the cavity, for two values of L, wave frequency $\omega = 1.008\ |\Omega_e|$, and other parameters as in Fig. 1. (a) $L = 400$ km; (b) $L = 300$ km.

Finally, we analyse the wave trajectories as a function of the cavity width. Fig. 9 shows the trajectories of a bunch of rays, in the $x - z$ plane, for $\omega = 1.008\ |\Omega_e|$ and $0.13 \leq N_{||} \leq 0.19$, for three values of the cavity width. The set of curves labelled by (a) has been obtained for the case of $L = 500$ km. It is seen that the rays are leaving the cavity region at an oblique angle relative to the direction of the magnetic field. However, the trajectories become more and more parallel to the magnetic field for decreasing L. For instance, case (b) is for $L = 400$ km and case (c) is for $L = 300$ km. In case (c), the rays are seen propagating nearly parallel to the walls of the cavity in the late stages of their trajectory, at the time when they suffer reabsorption according to panel (b) of Fig. 8. It must be said that for this case

of smaller cavity width the procedure adopted for the ray tracing has become less accurate in the prediction of the values of $N'_\perp$ when compared locally with the outcome of the dispersion relation, for both extremes of the $N_\parallel$ values considered, while keeping accuracy for the region $0.15 \leq N_\parallel \leq 0.17$. This decrease of accuracy in the ray tracing procedure is related to the violation of the condition $N''_\perp \ll N'_\perp$, when $N'_\perp$ is severely reduced in the case of nearly parallel propagation; it occurs in the final portion of the trajectory, when the wave energy has already been reabsorbed and nothing is really left of the ray, according to Fig. 8 (b).

Figure 7 (a)

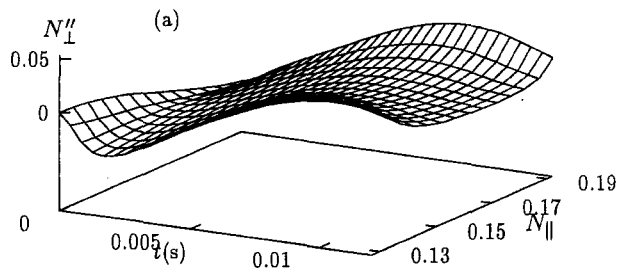

Figure 7 (b)

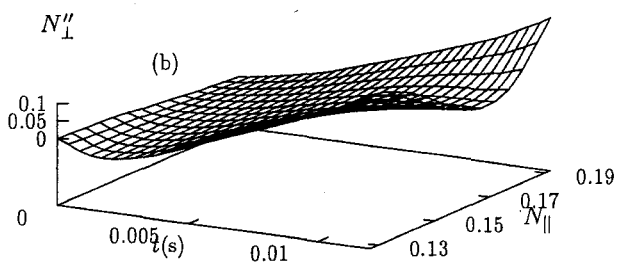

Figure 7. $N''_\perp$ as a function of the initial values of $N_\parallel$ and the time since the departure of the wave from the center of the cavity, for two values of L, wave frequency $\omega = 1.008\ |\Omega_e|$ and other parameters as in Fig. 1. (a) $L = 400$ km; (b) $L = 300$ km.

Figure 8 (a)

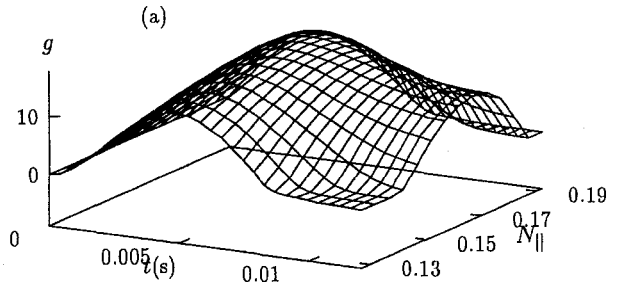

Figure 8 (b)

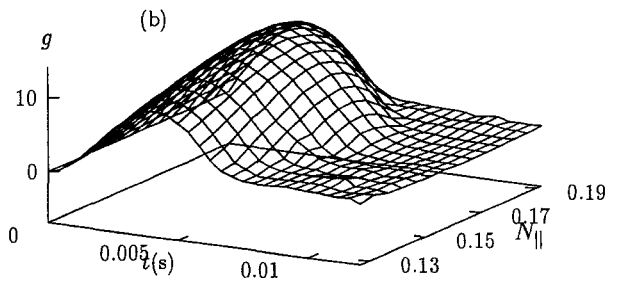

Figure 8. $g \equiv ln(I_\omega / I_{bb})$ as a function of the initial values of $N_\parallel$ and the time since the departure of the wave from the center of the cavity, for two values of L, wave frequency $\omega = 1.008\ |\Omega_e|$, and other parameters as in Fig. 1. (a) $L = 400$ km; (b) $L = 300$ km.

Figure 9

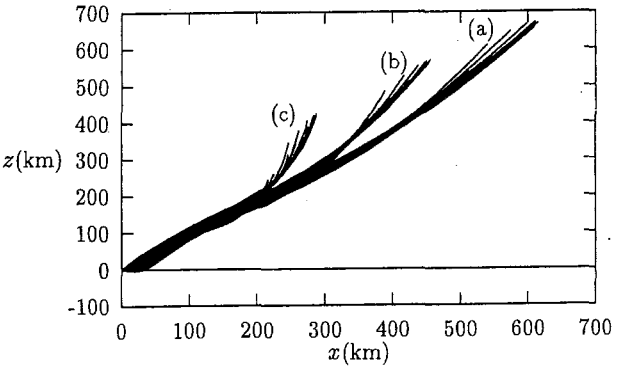

Figure 9. Ray trajectories in the $x - z$ plane, for $\omega = 1.008\ |\Omega_e|$ and $0.13 \leq N_\parallel \leq 0.19$. (a) $L = 500$ km; (b) $L = 400$ km; $L = 300$ km. Other parameters as in Fig. 1.

V. Summary and conclusions

In the present paper we developed the emission and amplification of fast extraordinary mode waves in finite

width auroral cavities. We resumed previous work on the subject, utilizing a formulation which incorporates relevant thermal and relativistic effects in the dispersion relation and in the geometric optics equations for the ray trajectories.

The intensity of radiation along the wave trajectories was evaluated with the use of the transfer equation. The cyclotron emissivity along the trajectory has been evaluated and integrated for several values of the cavity width. For the evaluation of the emissivity, we used a well known procedure which is based on the average value of the Poynting vector.

The auroral cavity was described by means of a two dimensional model which has already been utilized in previous studies. The electron population includes the effects of the cold electron population and an energetic population, with a generalized loss cone distribution function with a drift velocity parallel to the ambient magnetic field.

We have considered frequencies near electron cyclotron frequency, starting from a given position at the center of auroral cavities, with a range of values of $N_{||}$ for which there is significant local negative absorption coefficient. These rays were followed by means of the formalism of the geometric optics, and the outcome has qualitatively confirmed previous analysis which did not include the evaluation of the emissivity along the trajectories. We have obtained wave intensitities for the most amplified rays which are only nearly twice those obtained without taking into account the emissivity. The amplification suffered by these rays was seen to be significant, but still slightly below the necessary in order to account for the observed levels of AKR radiation. For the most amplified frequencies, we have observed that the reduction in the cavity size can be deleterious to the efficiency of the amplification, for the whole range of $N_{||}$ considered.

These results rely on several assumptions about the auroral cavity and about the electron distribution function. We have recently investigated the effect of a modification in the cavity profiles, demonstrating that the existence of depletions inside the auroral cavity can contribute to increase the wave amplification[24]. We intend to investigate in the near future the effect of the inclusion of other features in the distribution function, like the "bump" appearing in the actual electron distribution in the auroral zones, which has been suggested as a source of free energy for the AKR[2].

Acknowledgements

This work has been partially supported by the Brazilian agencies Conselho Nacional de Desenvolvimento Científico e Tecnológico (CNPq) and Financiadora de Estudos e Projetos (FINEP). We thank R. Gaelzer for useful comments and fruitful discussions. The numerical calculations have been partially made at the Supercomputer Center installed at the Universidade Federal do Rio Grande do Sul (CESUP-UFRGS).

References

1. C. S. Wu and L. C. Lee, Astrophys. J., **230**, 621 (1979).
2. P. Louarn, A. Roux, H. de Féraudy, D. LeQuéau, M. André and L. Matson, J. Geophys. Res., **95**, 5983 (1990).
3. A. Roux, A. Hilgers, H. de Feraudy, D. LeQuéau, P. Louarn and S. Perraut, J. Geophys. Res., **98**, 11657 (1993).
4. N. Omidi and D. A. Gurnett, J. Geophys. Res., **89**, 10801 (1984).
5. D. LeQuéau, R. Pellat and A. Roux, Annales Geophysicae, **3**, 273 (1985).
6. P. Zarka, D. LeQuéau and F. Genova, J. Geophys. Res., **91**, 13542 (1986).
7. A. Bahnsen, B. M. Pedersen, M. Jespersen, E. Ungstrup, L. Eliasson, J. S. Murphree, R. D. Elphinstone, L. Blomberg, G. Homgren and L. J. Zanetti, J. Geophys. Res., **94**, 6643 (1989).
8. H. K. Wong, C. S. Wu, F. J. Ke, R. S. Schneider and L. F. Ziebell, J. Plasma Phys., **28**, 502 (1982).
9. P. L. Pritchett, J. Geophys. Res., **89**, 8957 (1984).
10. P. L. Pritchett, Phys. Fluids, **29**, 2919 (1986).
11. D. LeQuéau, R. Pellat and A. Roux, J. Geophys. Res., **89**, 2831 (1984).
12. D. LeQuéau, R. Pellat and A. Roux, The Physics of Fluids, **27**, 247 (1984).
13. D. LeQuéau and P. Louarn, J. Geophys. Res., **94**, 2605 (1989).
14. P. L. Pritchett and R. M. Winglee, J. Geophys. Res., **94**, 129 (1989).

15. R. F. Benson and W. Calvert, Geophys. Res. Lett., **6**, 479 (1979).
16. W. Calvert, Geophys. Res. Lett., **8**, 919 (1981).
17. R. F. Benson, J. Geophys. Res., **90**, 2753 (1985).
18. A. Hilgers, H. de Feraudy and D. LeQuéau, J. Geophys. Res., **97**, 8381 (1992).
19. A. Hilgers, B. Holback, G. Holmgren and R. Boström, J. Geophys. Res., **97**, 8631 (1992).
20. W. Calvert, J. Geophys. Res., **87**, 8199 (1982).
21. P. L. Pritchett, J. Geophys. Res., **91**, 13569 (1986).
22. R. Gaelzer, L. F. Ziebell and R. S. Schneider, J. Geophys. Res., **97**, 19299 (1992).
23. R. Gaelzer, L. F. Ziebell and R. S. Schneider, J. Geophys. Res., **99**, 8905 (1994).
24. C. J. H. Cavalcanti, R. S. Schneider and L. F. Ziebell, J. Geophys. Res., **101**, 24557 (1996).
25. A. Hilgers, A. Roux and R. Lundin, Geophys. Res. Lett., **18**, 1493 (1991).
26. Y. T. Chiu and M. Schulz, J. Geophys. Res., **83**, 629 (1978).
27. Peter H. Yoon and Tom Chang, J. Plasma Phys., **42**, 193 (1989).
28. H. P. Freund and C. S. Wu, Phys. Fluids, **20**, 963 (1977).
29. H. P. Freund and C. S. Wu, Phys. Fluids, **20**, 1697 (1977).
30. Ira B. Bernstein, Phys. Fluids, **18**, 320 (1975).
31. William H. Press, Brian P. Flannery, Saul A. Teukolsky and William T. Vetterling, *Numerical Recipes - The Art of Scientific Computing*, Cambridge, Cambridge (1989).
32. G. Bekefi, *Radiation Processes in Plasmas*, John Wiley and Sons, New York (1966).
33. K. Audenaerde, Phys. Plasmas, **19**, 299 (1977).
34. M. Bornatici, R. Cano, O. de Barbieri and F. Engelmann, Nucl. Fusion, **23**, 1153 (1983).